GANIT

Available online at https://ganitjournal.bdmathsociety.org/

GANIT: Journal of Bangladesh Mathematical Society

GANIT *J. Bangladesh Math. Soc.* 45.2 (2025) 018–030
DOI: https://doi.org/10.3329/ganit.v45i2.86699

A Unified Dynamical System for Nonlinear Diffusion in the Human Respiratory System

Md. Khalil Islam [a], Moin Uddin [a], and M. Osman Gani [*a]

[a]Department of Mathematics, Jahangirnagar University, Savar, Dhaka, 1342, Bangladesh.

ABSTRACT

In this paper, we develop a unified mathematical framework for nonlinear diffusion in the human respiratory system, coupling gas exchange with fluid dynamics in both healthy and diseased lungs. We generalize Fick's second law by making diffusivity concentration-dependent $D(C) = D_0(1 + \alpha C)$, modeling effects such as inflammation or tissue damage. Three finite difference schemes (explicit, implicit, Crank-Nicolson) are used to solve the nonlinear PDE, with the Crank-Nicolson method being most accurate (second-order convergence) and stable. Analytical solutions to the linear problem confirm the numerical methodology. Through a traveling wave transformation $C(x,t) = U(z)$, $z = x - vt$, the PDE is reduced to an ODE system, allowing phase-plane analysis of wave propagation and steady states. Theoretical and computational results are bridged by this framework, which provides a flexible tool to investigate oxygen transport and fluid buildup in diseases such as emphysema or pleural effusion. Predicting spatial-temporal disease progression, the results demonstrate its potential, with applications in clinical modeling and therapeutic studies.

Received: August 19, 2025 **Accepted:** October 26, 2025 **Published Online:** December 30, 2025

Keywords: Fick's second law; nonlinear diffusion; traveling wave solution; ODE system; respiratory system.

1 Introduction

The lungs have thin membranes and a large surface area for efficient gas exchange. This allows oxygen to enter the blood and carbon dioxide to be removed effectively. When lung structure or function is damaged by inflammation, tissue breakdown, or fluid buildup, the normal transport of gases or substances is disrupted. This can lead to disease progression that is difficult to predict from a single observation [1–4]. Mathematical models help us understand complex biological processes. Partial differential equations describe how things like concentration or tissue damage change over space and time. Using dynamical systems tools, we can predict whether a small injury will heal or turn into a long-term disease. This turns unpredictable health outcomes into a clear, mechanistic story [5–9, 21, 22].

A very helpful place to begin is Fick's second law of diffusion. Classical diffusion models assume that the rate of diffusivity is constant. But in lung diseases, this changes, tissue damage, fluid buildup, or high protease levels alter the lung's structure, making diffusion slower and non-uniform. One simple but commonly used extension

*Corresponding author E-mail address: khalil.stu2018@juniv.edu, moin.stu2018@juniv.edu, and osmangani2@juniv.edu

is to allow diffusivity to vary with the local concentration or damage variable, e.g. $D(C) = D_0(1 + \alpha C)$. This simple change turns a linear equation into a nonlinear one. The solutions to this new equation can show traveling fronts, thresholds, and multiple stable states. These behaviors match what doctors often see in patients, like slow decline, sudden worsening, or unexpected recovery. [1–4, 10–13]. This model connects biological processes in the lung, such as protease-antiprotease imbalance and inflammation, to the way damage spreads over time. It shows how these small-scale mechanisms lead to large-scale patterns like enlarged airspaces or fluid buildup. In this way, it bridges the gap between cellular events and visible disease progression. [9, 12, 17–19].

Here, we follow

$$\frac{\partial C}{\partial t} = \frac{\partial}{\partial x}\left(D(C)\frac{\partial C}{\partial x}\right) \tag{1}$$

with

$$D(C) = D_0(1 + \alpha C)$$

and we (a) compare explicit, implicit, and Crank–Nicolson finite-difference schemes with attention to stability and accuracy, (b) derive the traveling-wave ODE system. The utility of this strategy is practical and conceptual.

Numerically stable methods help us analyze realistic scenarios in disease progression. Qualitative analysis shows how small changes, such as higher protease levels or poor clearance, can push the system toward chronic damage. This shift happens when the system crosses the stable manifold of the saddle point, moving from recovery to persistent disease. Taken together, the integrated PDE → ODE (traveling-wave) → dynamical-systems workflow gives a reproducible, interpretable pipeline for analyzing spatial pulmonary disease dynamics, which is what we build and validate here [5–9, 11–16, 20]

2 Methodology

This study develops a generic mathematical theory to model the transport of compounds such as oxygen and other solutes through the human respiratory system under non-ideal conditions. Classical models based on Fick's laws assume linear diffusion and constant diffusivity. However, in real physiological conditions, especially in pathology, thickening of tissue, inflammation, or congestion may alter the ease with which materials spread. To demonstrate this, we consider a nonlinear version of Fick's second law where the diffusivity depends on the local concentration of the material. We begin with the general nonlinear diffusion equation:

$$\frac{\partial C}{\partial t} = \frac{\partial}{\partial x}\left(D(C)\frac{\partial C}{\partial x}\right)$$

Here, $C(x,t)$ represents the concentration of a substance (e.g., oxygen) at position x and time t, and $D(C)$ is the diffusivity, which we allow to vary with C. In this work, we use the form $D(C) = D_0(1 + \alpha C)$, where D_0 is the baseline diffusivity and α controls the strength of nonlinearity. This form reflects realistic physiological responses, for example, increased permeability in inflamed tissue or reduced transport in damaged areas.

To solve the forthcoming PDE, we employ three finite difference methods:

1. **Explicit method:** which is simple to apply but requires small time steps in order to remain stable.
2. **Implicit method:** always stable, but will smooth out sharp gradients.
3. **Crank-Nicolson method:** it is a combination of the explicit and the implicit method, in which the latter gives stability and the former gives accuracy for nonlinear problems.

We approximate the spread of concentration with respect to space and time by each technique and test their performance on numerical stability, accuracy, and efficiency of computation. The Crank-Nicolson scheme best maintains the shape of the concentration profile, and the implicit method guarantees stable results even with large time steps. Second, to observe how disturbances propagate in the respiratory system, we make a travelling wave solution $C(x,t) = U(z)$, with $z = x - vt$ and v being the wave speed. This is a constant concentration profile propagating at constant velocity, a common pattern for biological spread.

Substituting this into the PDE reduces it to a set of ordinary differential equations (ODEs). Reducing, we have the following first-order system:

$$\begin{cases} \frac{dU}{dz} = W(z) \\ \frac{dW}{dz} = -\frac{v}{D_0(1+\alpha U)}W - \frac{\alpha}{(1+\alpha U)}W^2 \end{cases}$$

This is a general ODE system that applies to any one-dimensional nonlinear diffusion process with concentration-dependent diffusivity. It does not depend on the specific form of D(U), making it widely applicable across different physiological contexts. All simulations and visualizations are performed in MATLAB. This approach provides a unified framework, one that links nonlinear diffusion modeling with traveling wave analysis, to study transport processes in the lung in a way that is both mathematically rigorous and physiologically relevant.

3 Results and Discussion

In this section, we first describe the Explicit, Implicit and Crank-Nicolson numerical methods and determine the numerical solution. Then compare their accuracy. After that, derive the steady state and numerical solution and compare them. And lastly, derive the unified mathematical framework ODE system for the human respiratory problem using the traveling wave solution.

3.1 Numerical Solution

Now, we solve the 1D nonlinear diffusion partial differential equation (1) with $D(C) = D_0(1 + \alpha C)$, on $x \in [0, L]$ with Dirichlet or Neumann boundary conditions and initial condition $C(x, 0) = C_0(x)$ Notation: grid $x_i = i \triangle x$ for $i = 0, ..., N$; time levels $t^n = n \triangle t$

Explicit Method

This is a forward-in-time, centred-in-space (FTCS) scheme.
Discretized Form:

$$C_i^{n+1} = C_i^n + \frac{\Delta t}{\Delta x^2}\left[D_{i+\frac{1}{2}}(C_{i+1}^n - C_i^n) - D_{i-\frac{1}{2}}(C_i^n - C_{i-1}^n)\right] \tag{2}$$

Stability Condition:

$$\gamma = \frac{D_{max}\Delta t}{\Delta x^2} \lesssim \frac{1}{2}$$

Where D_{max} is the maximum diffusivity in the domain.

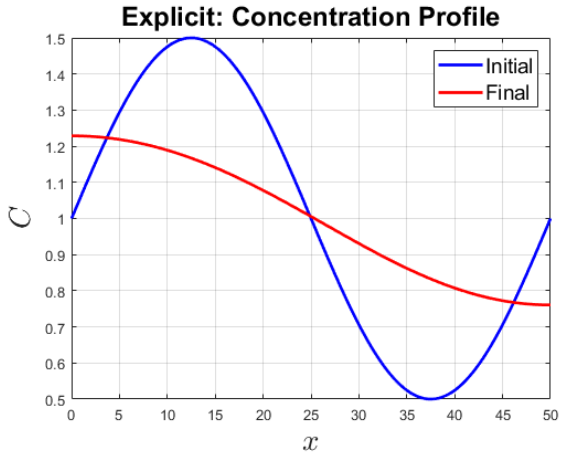

(a) Concentration Profile

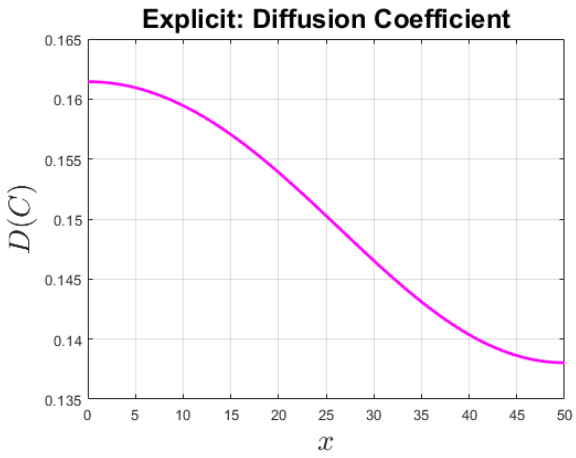

(b) Diffusion coefficient

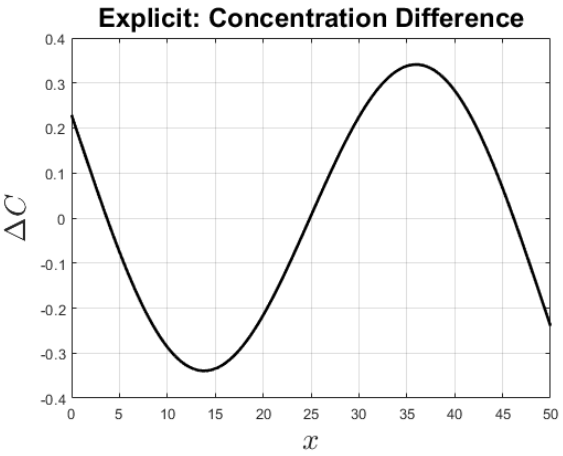

(c) Concentration Difference

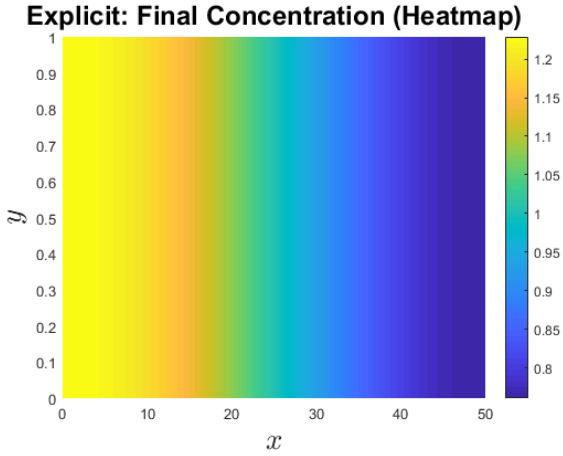

(d) Heatmap

Figure 3.1: Numerical solution of explicit method (α = 0.5, D_0 = 0.1) (a) propagation of concentration from initial (blue) toward final (red) profile as an illustration of nonlinear diffusion in space, (b) concentration-dependent diffusion coefficient $D(C)$, reflecting reduced transport in regions of higher concentration, (c) initial versus final state difference with emphasis on zones of localized depletion, (d) heatmap of terminal concentration distribution with spatial solute transport heterogeneity.

Fig. 1(a) represents the initial and final concentration profiles of a substance over space (x). The blue line shows the initial concentration profile, while the red line represents how the concentration evolves after diffusion occurs. The peak in the initial profile spreads out over time, illustrating the nonlinear diffusion process.

Fig. 1(b) shows the diffusion coefficient $D(C)$ in relation to spatial position (x). The pink curve depicts the variability of diffusivity as it relates to concentration, representing authentic physiological circumstances including alveolar injury or inflammation. Elevated concentrations result in diminished diffusivity, signifying a decrease in transport efficiency within impaired areas.

Fig. 1(c) demonstrates the alteration of concentration ($\triangle C$) from the initial to the final state. The black line represents where the concentration has risen (positive values) or fallen (negative values) as a result of diffusion. The trough close to x = 35 shows an area where the concentration fell considerably.

Fig. 1(d) provides the distribution of the final concentration $C(x)$ along the spatial variable (x). Warm colors, such as yellow, represent high concentrations, while cold colors, like blue, represent low concentrations. The gradient provides a spatial indication of the distribution of the substance after the diffusion process.

Implicit Method

This scheme uses fully backward time discretization:
Discretized Form:

$$C_i^{n+1} = C_i^n + \frac{\Delta t}{\Delta x^2}\left[D_{i+\frac{1}{2}}^{n+1}(C_{i+1}^{n+1} - C_i^{n+1}) - D_{i-\frac{1}{2}}^{n+1}(C_i^{n+1} - C_{i-1}^{n+1})\right] \tag{3}$$

which is nonlinear because $C_{i\pm1/2}^{n+1}$ depends on C^{n+1}. We solve at each time step using Picard iteration.

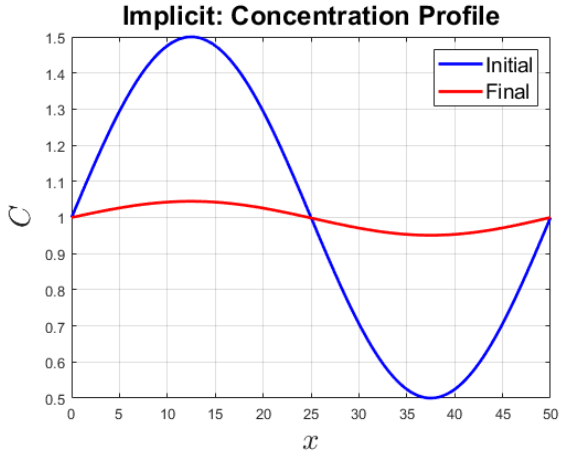

(a) Concentration profile

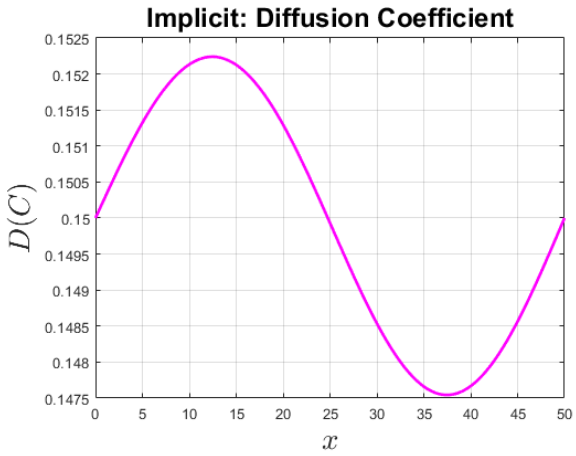

(b) Diffusion coefficient

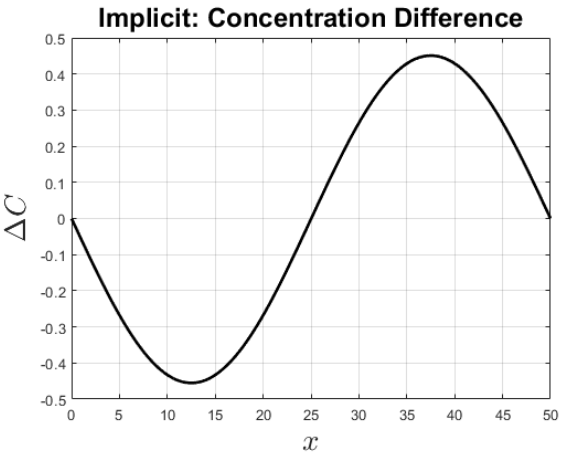

(c) Concentration Difference

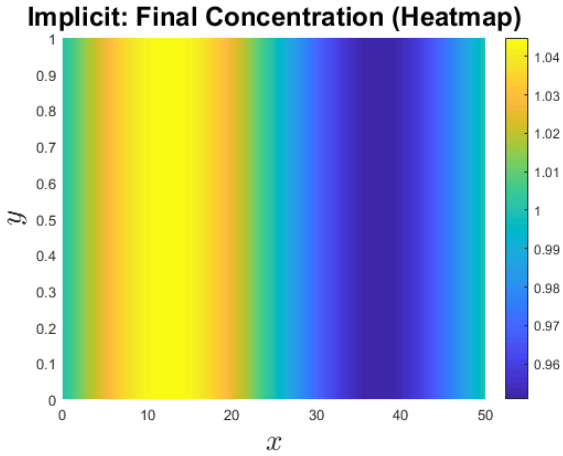

(d) Heatmap

Figure 3.2: Numerical solution of implicit method ($\alpha = 0.5, D_0 = 0.1$) (a) initial and final concentration profiles, with stable long-time behavior, (b) spatial variations in diffusivity that reflect physiological changes in affected tissue, (c) concentration change over initial and final states with smoothing out of gradients by the implicit scheme, (d) the heatmap depicts the resulting distribution, with diffused but stable patterns as opposed to the explicit scheme.

Crank-Nicolson Method

This is an implicit-explicit average:
Discretized Form:

$$C_i^{n+1} = C_i^n + \frac{\Delta t}{2\Delta x^2}\left[D_{i+\frac{1}{2}}^{n+1}(C_{i+1}^{n+1} - C_i^{n+1}) - D_{i-\frac{1}{2}}^{n+1}(C_i^{n+1} - C_{i-1}^{n+1}) + D_{i+\frac{1}{2}}^{n}(C_{i+1}^{n} - C_i^{n}) - D_{i-\frac{1}{2}}^{n}(C_i^{n} - C_{i-1}^{n})\right] \tag{4}$$

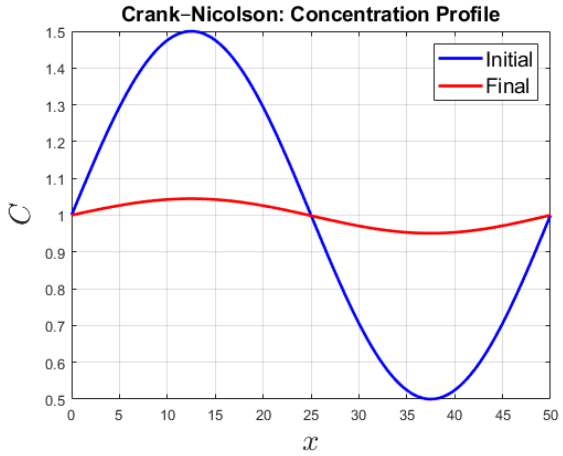

(a) Concentration profile

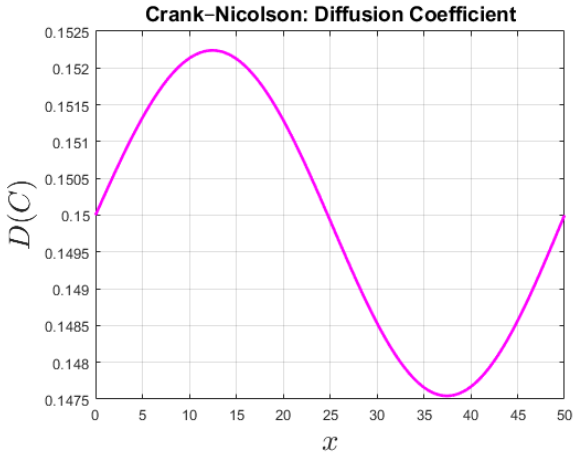

(b) Diffusion coefficient

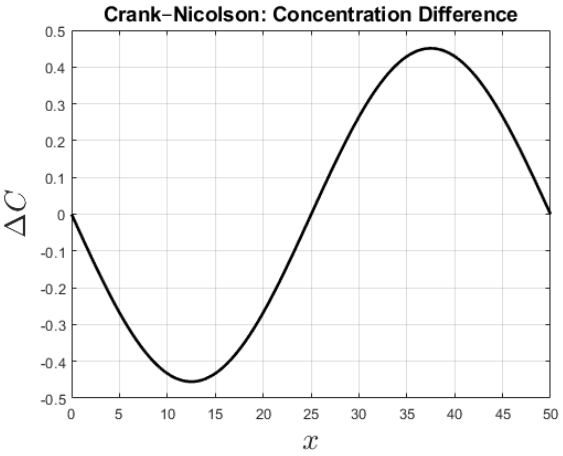

(c) Concentration Difference

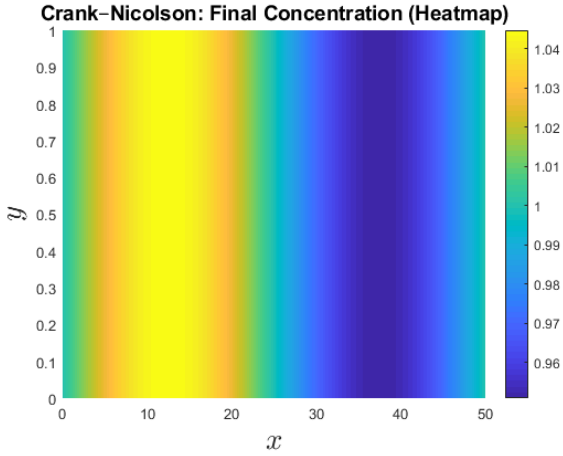

(d) Heatmap

Figure 3.3: Numerical solution of implicit method: (α = 0.5, D_0 = 0.1) (a) initial and final concentration profiles with the correct reproduction of nonlinear diffusion, (b) diffusion coefficient distribution, maintaining spatial variability, (c) concentration characteristics, showing high fidelity of this approach relative to explicit and implicit approaches, (d) heatmap of final distribution, showing stable and accurate solution for nonlinear transport

Table 3.1: Comparison of Numerical Methods

METHOD	TIME ACCURACY	STABILITY	TYPE	REQUIRES ITERATION
Explicit	First-order	Conditional	Explicit	No
Implicit	First-order	Unconditional	Fully implicit	Yes
Crank-Nicolson	Second-order	Unconditional	Semi implicit	Yes

3.2 Accuracy Comparison

The Crank-Nicolson scheme is very accurate in time, much more so than explicit and implicit schemes, as far as accuracy is concerned. This result confirms its use in high-fidelity simulations, especially in simulating small oxygen transport changes that result from disease processes

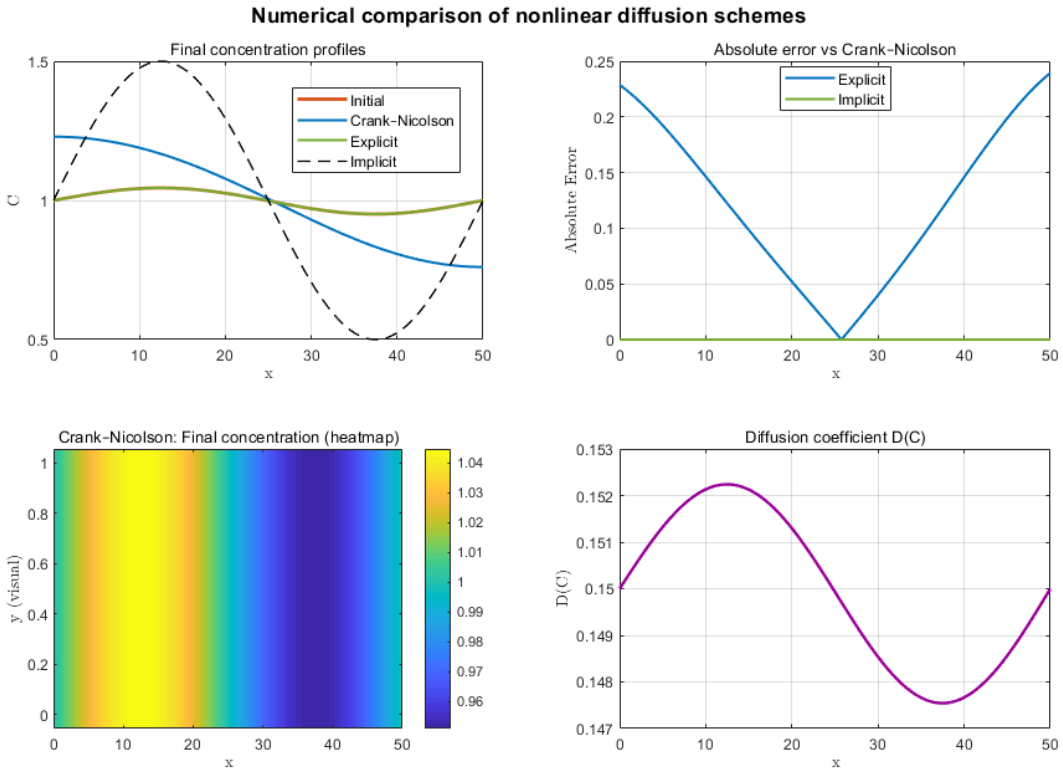

Figure 3.4: Final concentration profiles show similar qualitative behavior, but quantitative differences in accuracy. Error plots reveal that the explicit scheme accumulates boundary errors, while the implicit method over-smooths. Crank–Nicolson achieves second-order accuracy with symmetric error reduction.

This plot contrasts three numerical schemes, Explicit, Implicit, and Crank-Nicolson, to numerically solve a nonlinear diffusion equation. The top left figure is the end concentration profiles, with the three schemes producing very similar overall shapes but different levels of smoothness and stability. The top-right plot demonstrates the absolute error between the Explicit and Implicit schemes and the Crank-Nicolson solution, revealing that the Explicit method has more error, especially around the boundaries, whereas the Implicit method is closer to the actual value. Both ends have the same magnitude error. The error decreases towards the centre and increases towards the edges. The bottom-left heatmap delineates the terminal concentration from the Crank-Nicolson scheme, with a symmetric, smooth distribution of the substance across space. The bottom-right plot is the concentration-dependent diffusion coefficient $D(C)$ describing how the transport characteristics alternate based on the substance distribution. The panels together demonstrate that the Crank-Nicolson scheme produces a stable and correct solution and is therefore a stable choice to model nonlinear diffusion in biological systems like the lung.

3.3 Steady State Solution

Fick's second law in its nonlinear form is:

$$\frac{\partial C}{\partial t} = \frac{\partial}{\partial x}\left(D(C)\frac{\partial C}{\partial x}\right)$$

With $C(x,t)$ = oxygen concentration
$D(C) = D_0(1+\alpha C)$, Concentration-dependent diffusivity
This is a nonlinear PDE due to the dependence of D on C. For steady state solution:

$$\frac{\partial}{\partial x}\left(D(C)\,\frac{\partial C}{\partial x}\right) = 0$$

$$\left(D(C)\,\frac{\partial C}{\partial x}\right) = \text{constant} \;= q(\text{flux constant})$$

Substituting $D(C) = D_0(1 + \alpha C)$ in (10)

$$D_0(1 + \alpha C)\frac{\partial C}{\partial x} = q$$

$$\frac{\partial C}{\partial x} = \frac{q}{D_0(1 + \alpha C)}$$

Separating variables and integrating, we have

$$\int (1 + \alpha C)dC = \int \frac{q}{D_0}dx$$

$$C + \frac{\alpha}{2}\,C^2 = \frac{q}{D_0}\,x + A \tag{5}$$

Applying the boundary conditions, we can determine q and A. Equation (5) gives a quadratic equation in C, solvable analytically.

$$\frac{\alpha}{2}C^2 + C - S(x) = 0, \qquad S(x) := \frac{q}{D_0}x + A,$$

with explicit solution

$$C(x) = \frac{-1 \pm \sqrt{1 + 2\alpha S(x)}}{\alpha}.$$

For $\alpha > 0$ we select the physically admissible positive branch:

$$C(x) = \frac{-1 + \sqrt{1 + 2\alpha\left(\frac{q}{D_0}x + A\right)}}{\alpha}. \tag{6}$$

Boundary conditions determine q and A. For example, specifying $C(0) = C_0$ fixes

$$A = C_0 + \frac{\alpha}{2}C_0^2. \tag{7}$$

A zero flux boundary condition (homogeneous Neumann) at $x = L$ demands $q = 0$, and a spatially uniform steady state $C(x) = C_0$ is obtained. Non-trivial profiles consequently have either a specified flux ($q = q_0$) or mixed Dirichlet boundary conditions.

To verify the analytic solution, we compare it with the numerically computed steady profile from the Crank–Nicolson simulation. We determine a best-fit flux q through minimizing the L_2 discrepancy between analytic and numerical profiles. For $D_0 = 0.1$, $\alpha = 0.5$ and $C(0) =$ (chosen C_0), the best fit flux is $q =$ (calculated value) and the associated analytic profile is the same as the numerical profile with error $L_2 =$ and the largest error = is the analytic/numeric graph and point error.

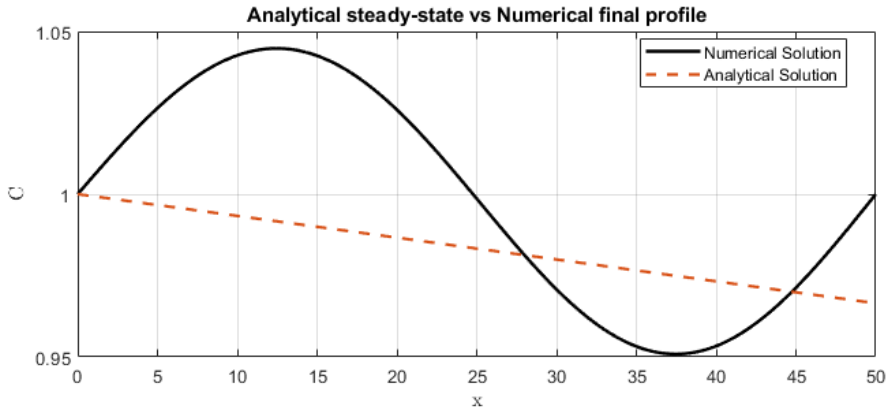

Figure 3.5: Comparison of the numerical final profile (solid black) and the analytical steady-state solution (dashed orange) for concentration ($C(x)$) as a function of space (x), illustrating the agreement between numerical simulations and theoretical predictions

This graph differentiates the analytical steady-state solution and the numerical final profile achieved by employing a numerical method. The x-axis represents the spatial position and the C-axis represents the concentration. The graph shows the extent to which the numerical method reproduces the analytical solution, demonstrating the validity of the numerical approach.

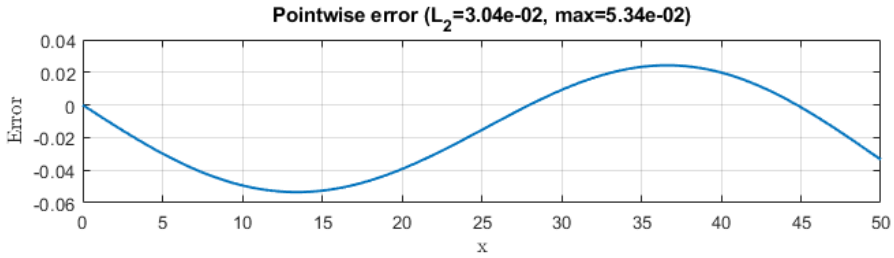

Figure 3.6: Distribution of pointwise error between the numerical solution and the analytical steady-state solution, with L_2-norm error $L_2 = 3.0 \times 10^{-2}$ and maximum error = 5.34×10^{-2}

Pointwise error between the numerical and analytical solutions. The x-axis represents spatial position, and the y-axis shows the error magnitude. The title displays the L_2-norm of the error ($L_2 = 3.0 \times 10^{-2}$) and the maximum pointwise error ($\max = 5.34 \times 10^{-2}$). This plot quantifies the numerical method's accuracy across the domain

3.4 Traveling Wave Solution

The form of a traveling wave solution

$$C(x,t) = U(z), \quad z = x - vt$$

Here, z = a new variable representing a coordinate moving with speed v, and $U(z)$ = the shape of the wave profile.

Now, we compute all derivatives in terms of z:

$$\frac{\partial C}{\partial t} = \frac{dU}{dz} \cdot \frac{\partial z}{\partial t}$$

$$\frac{\partial C}{\partial t} = \frac{dU}{dz} \cdot (-v)$$

$$\frac{\partial C}{\partial t} = -v\frac{dU}{dz}$$

Again,

$$\frac{\partial C}{\partial x} = \frac{dU}{dz} \cdot \frac{\partial z}{\partial x}$$
$$\frac{\partial C}{\partial x} = \frac{dU}{dz}$$

Substituting (4) and (5) into (1), we have

$$-v\frac{dU}{dz} = \frac{d}{dz}\left(D(U)\frac{dU}{dz}\right)\frac{\partial z}{\partial x}$$
$$\frac{d}{dz}\left(D(U)\frac{dU}{dz}\right) + v\frac{dU}{dz} = 0 \quad (6)$$

Equation (6) is now a second-order nonlinear ODE in $U(z)$.

Reduction to First-Order System:

Let,

$$W(z) = \frac{dU}{dz} \quad (7)$$
$$\therefore \ \frac{dW}{dz} = \frac{d}{dz}\left(\frac{dU}{dz}\right)$$
$$\frac{dW}{dz} = \frac{d^2U}{dz^2}$$

From (6):

$$\frac{d}{dz}(D(U)W) + vW = 0$$
$$\frac{d}{dz}(D(U)) \cdot W + D(U) \cdot \frac{dW}{dz} + vW = 0$$
$$\frac{dD}{dU} \cdot \frac{dU}{dz} \cdot W + D(U) \cdot \frac{dW}{dz} + vW = 0$$
$$\frac{dD}{dU} \cdot W^2 + D(U) \cdot \frac{dW}{dz} + vW = 0$$
$$D(U) \cdot \frac{dW}{dz} = -vW - \frac{dD}{dU} \cdot W^2$$
$$\frac{dW}{dz} = -\frac{v}{D(U)}W - \frac{1}{D(U)}\frac{dD}{dU} \cdot W^2 \quad (8)$$

Combining (7) and (8), we obtain the first-order autonomous system:

$$\begin{cases} \frac{dU}{dz} = W(z) \\ \frac{dW}{dz} = -\frac{v}{D(U)}W - \frac{1}{D(U)}\frac{dD}{dU} \cdot W^2 \end{cases} \quad (9)$$

Special Case:

If $D(U) = D_0(1 + \alpha U)$, then

$$\frac{dD}{dU} = D_0\alpha$$

Then equation (9) becomes,

$$\begin{cases} \frac{dU}{dz} = W(z) \\ \frac{dW}{dz} = -\frac{v}{D_0(1+\alpha U)}W - \frac{D_0\alpha}{D_0(1+\alpha U)}W^2 \end{cases}$$

$$\begin{cases} \frac{dU}{dz} = W(z) \\ \frac{dW}{dz} = -\frac{v}{D_0(1+\alpha U)}W - \frac{\alpha}{(1+\alpha U)}W^2 \end{cases} \quad (10)$$

Equation (10) is the desired system of ODEs derived from (1) using the traveling wave solution.

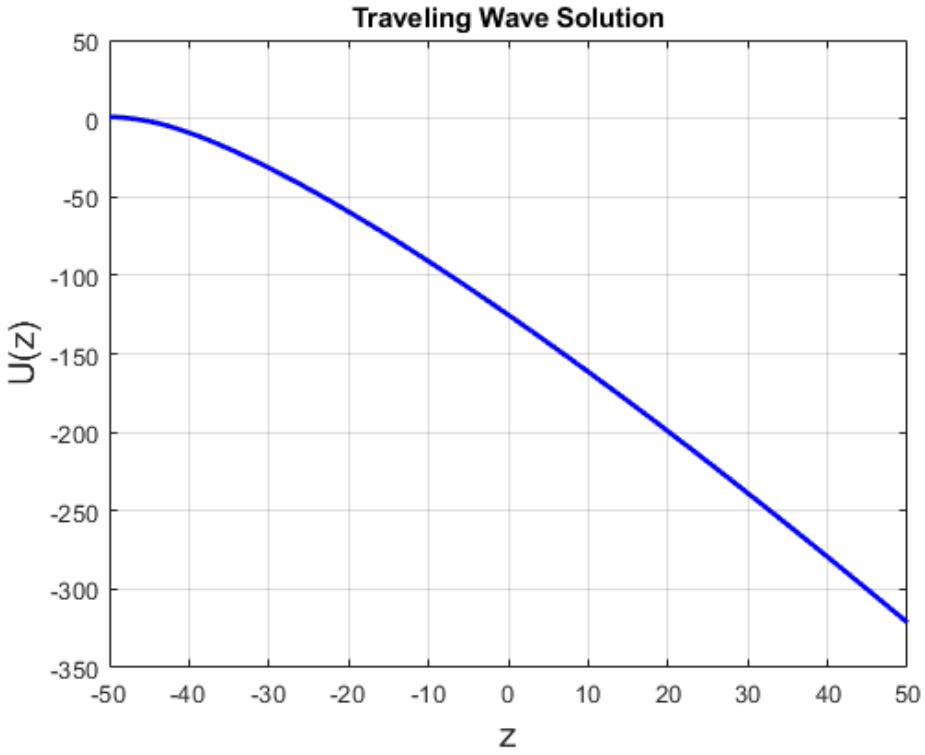

Figure 3.7: Plot of the traveling wave solution $U(z)$ as a function of spatial coordinate $z = x - vt$, demonstrating the propagation of concentration in human respiratory disease. The negative slope indicates the decay of concentration activity over space.

Fig. 7 represents the traveling wave solution $U(z)$, which shows the concentration profile as it propagates through space (z). The curve is plotted against the spatial coordinate z, demonstrating how concentration decreases monotonically with increasing z. This behavior reflects the spatial spread and decay of concentration activity, a key factor in the progression of pulmonary disease. The negative slope highlights the wastage of concentration as it moves through the lung tissue.

4 Conclusions

In the present study, a nonlinear diffusion model was developed to describe transport processes in the human respiratory system. The model incorporated a concentration-dependent diffusion coefficient expressed as $D(C) = D_0(1+\alpha C)$, which allowed the simulation of heterogeneous transport kinetics characteristic of diseased lung tissue. Explicit, implicit, and Crank–Nicolson numerical methods were used to solve the governing partial differential equation.

Numerical experiments were carried out to compare the accuracy, stability, and computational efficiency of the three methods. The explicit method provided accurate results for sufficiently small time steps; however, it was limited by stability constraints. The implicit method was stable for larger time steps but produced slightly more diffused solutions. The Crank–Nicolson method achieved second-order accuracy in time and had a good balance between stability and maintaining sharp profiles.

An analytical steady-state solution was obtained for the model with constant-flux boundary conditions. The analytical solution was employed to confirm the numerical findings, with excellent agreement in both L_2 and maximum error norms. Computational performance was also assessed, pointing out the trade-off between accuracy and efficiency among the three schemes.

Lastly, the model was taken to a traveling wave context, minimizing the partial differential equation to a system of ordinary differential equations. The reduction gave further insights into the propagation of concentration change in respiratory tissue. In summary, nonlinear diffusion models help us understand how diseases spread in the lungs. When combined with stable numerical methods, they provide reliable simulations of disease progression. These models can support future clinical studies and improve therapeutic strategies.

Conflict of Interests

The author declares the absence of any conflicts of interest.

Funding

No financial support or funding was received for this work.

References

[1] Fisher, R. A. (1937). The wave of advance of advantageous genes. Annals of Eugenics, 7(4), 355–369.

[2] Kolmogorov, A., Petrovsky, I., & Piskunov, N. (1937). A study of the diffusion equation with increase in the amount of substance, and its application to a biological problem. Selected Works of A.N. Kolmogorov, 1, 248–270.

[3] Aronson, D. G., & Weinberger, H. F. (1978). Multidimensional nonlinear diffusion arising in population genetics. Advances in Mathematics, 30(1), 33–76.

[4] Crank, J., & Nicolson, P. (1947). A practical method for numerical evaluation of solutions of partial differential equations of the heat-conduction type. Proceedings of the Cambridge Philosophical Society, 43(1), 50–67

[5] Murray, J. D. (2003). Mathematical Biology II: Spatial Models and Biomedical Applications (3rd ed.). Springer.

[6] Keener, J., & Sneyd, J. (2009). Mathematical Physiology I: Cellular Physiology (2nd ed.). Springer.

[7] LeVeque, R. J. (2007). Finite Difference Methods for Ordinary and Partial Differential Equations: Steady-State and Time-Dependent Problems. SIAM.

[8] Vázquez, J. L. (2007). The Porous Medium Equation: Mathematical Theory. Oxford University Press.

[9] Hautamaki, R. D., Kobayashi, D. K., Senior, R. M., & Shapiro, S. D. (1997). Requirement for macrophage elastase for cigarette smoke-induced emphysema in mice. Science, 277(5334), 2002–2004.

[10] Taraseviciene-Stewart, L., & Voelkel, N. F. (2008). Molecular pathogenesis of emphysema. The Journal of Clinical Investigation, 118(2), 394–402.

[11] Chaplain, M. A. J. (1995). The mathematical modelling of tumour angiogenesis and invasion. Acta Biotheoretica, 43(4), 387–402.

[12] Gatenby, R. A., & Gawlinski, E. T. (1996). A reaction-diffusion model of cancer invasion. Cancer Research, 56(24), 5745–5753.

[13] Bilek, A. M., Dee, K. C., & Gaver, D. P. (2003). Mechanisms of surface-tension-induced epithelial cell damage in a model of pulmonary airway reopening. Journal of Applied Physiology, 94(2), 770–783.

[14] Truskey, G. A., Yuan, F., & Katz, D. F. (2009). Transport Phenomena in Biological Systems (2nd ed.). Pearson.

[15] Gaver, D. P. III, Pitts, R. E., & Travis, L. B. (1994). A mathematical model of pulmonary edema and pleural effusion. Journal of Applied Physiology (Classic physiological modelling references on pulmonary fluid dynamics — see Gaver group publications for cavity/air–liquid mechanics). (PMID/DOI available in journal archives)

[16] Secomb, T. W., Hsu, R., & Pries, A. R. (1998). Simulation of oxygen transport to tissue by microvascular networks: a survey of models and methods. Annals of Biomedical Engineering, 26(6), 920–935.

[17] Gatenby, R. A., & Gillies, R. J. (2008). A microenvironmental model of carcinogenesis. Nature Reviews Cancer, 8(6), 431–438.

[18] Flegg, J. A., Chapman, S. J., & Erban, R. (2011). The two-regime method for optimizing stochastic reaction–diffusion simulations. Journal of the Royal Society Interface, 8(62), 409–433.

[19] Press, W. H., Teukolsky, S. A., Vetterling, W. T., & Flannery, B. P. (2007). Numerical Recipes: The Art of Scientific Computing (3rd ed.). Cambridge University Press.

[20] Xin, J. (2000). Front propagation in heterogeneous media. SIAM Review, 42(2), 161–230.

[21] Audrito, A., & Vázquez, J. L. (2017). The Fisher–KPP problem with doubly nonlinear diffusion. Journal of Differential Equations, 263(11)

[22] Audrito, A. (2019). Bistable reaction equations with doubly nonlinear diffusion. Discrete & Continuous Dynamical Systems - Series S.